



Gravity waves and momentum fluxes in the mesosphere and lower thermosphere using 430 MHz dual-beam measurements at Arecibo:

2. Frequency spectra, momentum fluxes, and variability

David C. Fritts,¹ Diego Janches,¹ Dennis M. Riggin,¹ Robert G. Stockwell,¹ Michael P. Sulzer,² and Sixto Gonzalez²

Received 10 November 2005; revised 23 May 2006; accepted 26 June 2006; published 28 September 2006.

[1] Janches et al. (2006) described a new dual-beam use of the 430 MHz incoherent scatter radar at the Arecibo Observatory in Puerto Rico. We found the technique to define the radial wind field in the mesosphere and lower thermosphere with sufficient accuracy to characterize gravity waves occurring at high frequencies and small spatial scales over an extended altitude range. The coplanar, dual-beam experiment was also designed to test the ability of the system to measure gravity wave momentum fluxes and their frequency distributions, and we report here on those results. Initial measurements were of limited duration and necessarily represent a case study, but they demonstrate the value of such measurements for studies of GW variability and large-scale interactions. Radial velocity variances reveal preferential eastward propagation for most intervals and altitudes, with the greatest propagation bias at lower altitudes and later times on 11 September when strong westward mean winds favor strong gravity filtering. The momentum fluxes observed during this experiment had ~ 50 -min averages that were often near zero, occasionally achieved amplitudes of ~ 20 to $50 \text{ m}^2 \text{ s}^{-2}$, displayed significant consistency in altitude, and exhibited an approximate anticorrelation with the zonal wind field in cases with significant momentum fluxes. Frequency spectra defined the major contributions to the momentum fluxes, while S transforms were employed to examine the temporal variability of the GWs and momentum fluxes in greater detail.

Citation: Fritts, D. C., D. Janches, D. M. Riggin, R. G. Stockwell, M. P. Sulzer, and S. Gonzalez (2006), Gravity waves and momentum fluxes in the mesosphere and lower thermosphere using 430 MHz dual-beam measurements at Arecibo: 2. Frequency spectra, momentum fluxes, and variability, *J. Geophys. Res.*, *111*, D18108, doi:10.1029/2005JD006883.

1. Introduction

[2] Janches et al. [2006] provided an extensive discussion of previous measurements of gravity waves (GWs) using the Arecibo Observatory (AO) 430 MHz incoherent scatter radar (ISR) and of the motivation for more quantitative GW studies in the mesosphere and lower thermosphere (MLT). Our intent here is to review our understanding of GW momentum flux measurements and MLT effects and to articulate the need for more specific and detailed momentum flux studies in the MLT. This paper will then demonstrate a promising new capability for such studies using the data obtained with the AO ISR and described by Janches et al. [2006].

[3] GW momentum fluxes, primarily the vertical flux of horizontal momentum, $\rho_0(z)\langle u'w' \rangle$ (where $\rho_0(z)$ is mean density and brackets denote a spatial and/or temporal

average) have been recognized to play a role in atmospheric dynamics for almost 40 years [Booker and Bretherton, 1967; Bretherton, 1969; Chunchuzov, 1971; Lilly, 1972]. It was not appreciated until much more recently, however, how significant and pervasive a role this has proven to be. Indeed, there remain key pieces to the puzzle that are understood poorly or not at all at present. It is beyond the scope of this paper to review all of the effects of GW momentum transport throughout the atmosphere. We will instead highlight what are thought to be the major roles, and the major uncertainties, in the MLT and direct the reader to the review by Kim et al. [2003] for a review of GW effects at lower altitudes.

[4] The dominant influences of GWs on the mean circulation and thermal structure in the MLT were noted by Janches et al. [2006] and include mesospheric jet closure, a GW-driven residual (meridional and vertical) circulation, and the induced cold summer mesopause and warm winter mesosphere, and GW momentum transport and deposition were identified as the major cause of these. Other influences were also noted in which GW momentum flux and divergence are not the dominant process. It is GW momentum transport and deposition, however, that is anticipated to (1) influence tidal and planetary wave (PW) amplitudes and

¹Colorado Research Associates, NorthWest Research Associates, Boulder, Colorado, USA.

²Arecibo Observatory, National Astronomy and Ionosphere Center, Arecibo, Puerto Rico.

phases due to GW filtering; (2) map the spatial and temporal character of these motions to higher altitudes where the remaining GWs are dissipated; (3) act as a local source of additional GW motions; and (4) provide episodic, and likely systematic, forcing of the thermosphere to much higher altitudes that is expected to exhibit a solar cycle modulation [Djuth *et al.*, 2004; Vadas and Fritts, 2004, 2005, 2006] (also see Fritts and Alexander [2003] for a review of these influences and extensive references to earlier studies). Indeed, mean forcing is reasonably well understood on the basis of the zonal mean circulation and thermal structure, and it is these GW interactions with tides and PWs and the variability in their excitation, occurrence, and responses that are of greatest interest here.

[5] Because of the important role of GW momentum transport and momentum flux divergence in the MLT, a number of techniques have been employed to measure these quantities. The seminal study was performed by Vincent and Reid [1983], who introduced the dual-beam technique which has provided the motivation for many additional studies as well as instrument and experimental designs (including ours). These authors recognized that the velocity covariance, $\langle u'w' \rangle$, can be estimated from the difference in radial velocity variances at two viewing angles inclined at equal and opposite angles off-zenith in a vertical plane as $\langle u'w' \rangle = (\langle V_E^2 \rangle - \langle V_W^2 \rangle) / 2 \sin(2\theta)$, where $\langle V_E^2 \rangle$ and $\langle V_W^2 \rangle$ are the velocity variances in beams inclined at an angle θ east and west from zenith, averaged over a suitable interval of time (or space), and the GW field contributing the momentum flux can be assumed to be statistically the same in the two beams throughout the averaging interval or volume. The great advantage of this method is that instruments that both measure radial velocities and resolve the range (e.g., Doppler radars and lidars) can provide altitude profiles of momentum flux, and thus also compute the momentum flux divergence with altitude.

[6] The dual-beam method has been employed to measure GW momentum fluxes in the MLT at a number of sites, including the MF radar at Adelaide, Australia [Vincent and Reid, 1983; Reid and Vincent, 1987; Fritts and Vincent, 1987; Murphy and Vincent, 1998], the SOUSY VHF radar at Andenes, Norway [Reid *et al.*, 1988], the VHF radar at Poker Flat, Alaska [Fritts and Yuan, 1989; Wang and Fritts, 1990, 1991], the MU VHF radar at Shigaraki, Japan [Tsuda *et al.*, 1990], the Jicamarca VHF radar near Lima, Peru [Fritts *et al.*, 1992; Hitchman *et al.*, 1992], the sodium lidar at the Starfire Optical Range near Albuquerque, New Mexico (C. S. Gardner and A. Z. Liu, Seasonal variations of vertical heat, Na, and momentum fluxes and their relationships to gravity wave activity and atmospheric stability in the mesopause region at Starfire Optical Range, NM, submitted to *Journal of Geophysical Research*, 2006), and the sodium lidar at the ALOMAR observatory at Andenes, Norway. This technique also inspired the construction of two large “Mill’s cross” MF radar arrays at Andenes, Norway and Pontianak, Indonesia (W. Singer, personal communication, 2002; B. Vincent, personal communication, 2002), but these systems have yet to yield momentum flux measurements. Despite their very different characteristics, the operational instruments have all yielded mean momentum fluxes (per unit mass) of ~ 5 to $15 \text{ m}^2 \text{ s}^{-2}$, and inferred

mean zonal accelerations up to $\sim 100 \text{ ms}^{-1} \text{ day}^{-1}$, depending on altitude, latitude, and season, with the direction of the mean acceleration opposed to the mean motion in virtually all cases. Some of these same studies also measured much larger momentum fluxes, as high as ~ 30 to $60 \text{ m}^2 \text{ s}^{-2}$, for intervals of ~ 1 to 8 hours [Fritts and Vincent, 1987; Reid *et al.*, 1988; Fritts and Yuan, 1989; Fritts *et al.*, 1992]. The measured mean values largely confirm the magnitudes of the GW drag introduced in middle atmosphere models through various GW parameterization schemes [McLandress, 1998; Kim *et al.*, 2003]. The much larger local values, however, are suggestive of strong tidal interactions [Fritts and Vincent, 1987; Wang and Fritts, 1991] and/or a potential for strong local body forcing in response to large-amplitude, spatially localized GW packets.

[7] The success of the dual-beam technique, and the obvious importance of GWs in forcing the mean and variable structure of the MLT, have also motivated a number of other techniques for momentum flux estimates. These include estimates based on chaff measurements of horizontal and vertical velocities [Meyer *et al.*, 1989], intensity variances in airglow [Gardner *et al.*, 1999; Swenson *et al.*, 1999; Tang *et al.*, 2002; Espy *et al.*, 2004, 2005], use of airglow and radar winds to estimate GW amplitudes and scales directly [Fritts *et al.*, 2002], satellite measurements of the departure of the mean state from uniform zonal flow and/or radiative equilibrium conditions [Smith and Lyjak, 1985; Smith, 1996], and CRISTA measurements of vertical and horizontal variations in temperature in sublimb viewing enabling GW momentum fluxes estimates [Ern *et al.*, 2004]. Several of these studies also suggest a potential for local momentum fluxes to be considerably larger than mean values as well as short-term radar averages.

[8] Our purpose in this paper is to examine the ability of the new AO 430 MHz ISR measurement capability described by Janches *et al.* [2006] for estimating GW momentum fluxes, their spatial and temporal variability, their frequency dependence, and their correlations with the larger-scale motion field in the MLT. The data collection and analysis methods were described in detail by Janches *et al.* [2006] and will not be repeated here. We first explore the \sim hourly averaged momentum fluxes and compare them with the \sim hourly averaged zonal winds in section 2. This will provide insights into the dynamics that control GW propagation, filtering, and the correlations observed between GW momentum fluxes and large-scale winds at a number of sites. To understand those components of the GW spectrum that contribute primarily to the momentum fluxes, we then compute and compare the radial velocity frequency spectra for those altitude and time intervals for which significant momentum fluxes were observed in section 3. Section 4 employs these data to examine the frequency spectra of the momentum fluxes on each day for those times and altitudes where significant fluxes were observed. We then probe the temporal behavior and the frequency content of both the radial velocities and the zonal momentum fluxes employing the S transform methodology [Stockwell *et al.*, 1996] to develop a more quantitative view of the GWs that contribute the major momentum fluxes, their propagation anisotropy, and their spatial and temporal

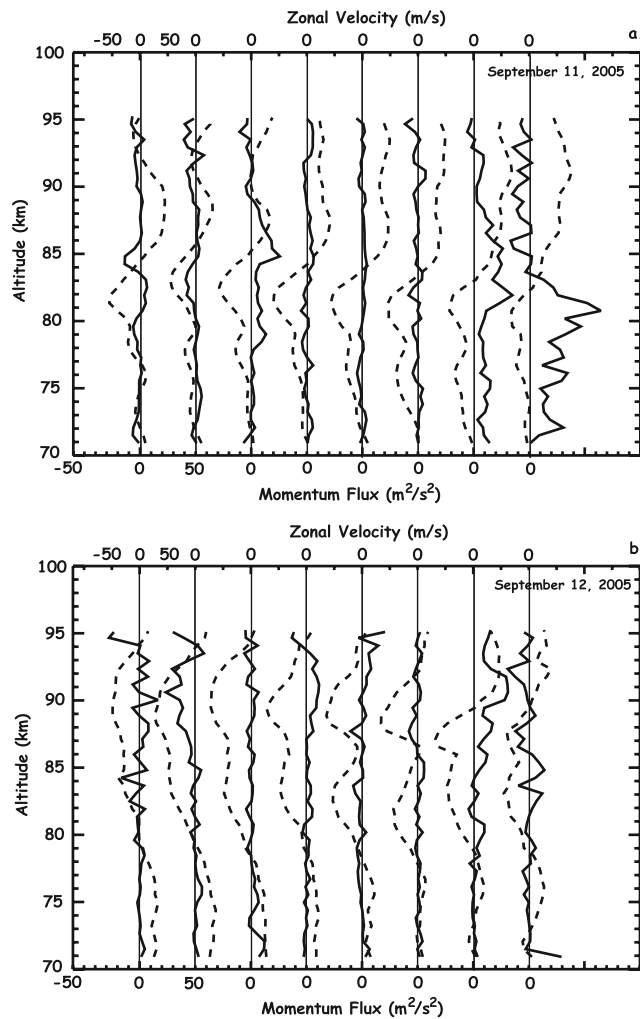


Figure 1. Zonal winds (dashed lines, top axes) and momentum fluxes (solid lines, bottom axes) from 71 to 95 km based on ~ 50 -min radial wind measurements employing beams inclined 15° east and west of zenith on (a) 11 and (b) 12 September 2005. Successive profiles are displaced by 100 ms^{-1} in velocity and $50 \text{ m}^2 \text{ s}^{-2}$ in momentum flux.

intermittency in section 5. Our discussion, summary, and conclusions are provided in section 6.

2. Hourly Momentum Fluxes

[9] Momentum flux profiles estimated from ~ 50 -min data intervals from 71 to 95 km on 11 and 12 September 2005, together with the zonal winds for the same intervals, are shown in Figure 1. These profiles reveal significant variability of the GW momentum fluxes with time and altitude. Importantly, however, 10 of these 16 profiles (see profiles 1, 2, 4, 5, and 6 in Figure 1a, and profiles 1 and 3–6 in Figure 1b) have very small momentum flux estimates over the majority of the altitude range. Essentially, independent (unsmoothed) estimates at adjacent altitudes are typically within a few $\text{m}^2 \text{ s}^{-2}$, especially where these fluxes are essentially zero. This is also true where momentum flux estimates depart significantly from zero, and where it is also

found that independent (but adjacent) altitude estimates vary by much less than their mean values. This suggests that radial velocity uncertainties lead to small statistical momentum flux uncertainties for ~ 50 -min estimates, and thus that these data are of sufficiently high quality to permit reliable momentum flux measurements, even for these relatively short intervals, when momentum flux estimates are significantly above these noise levels. These estimates also serve as further confirmation of small radial velocity uncertainties of $\sim 1 \text{ ms}^{-1}$ claimed by *Janches et al.* [2006], given the dependence of momentum flux estimates on radial velocity variances above. The ~ 7 -hour mean zonal winds and momentum fluxes obtained by averaging the individual profiles and smoothing the momentum flux profiles over 3 km (as this is approximately the smallest GW scale that should contribute to momentum flux variability with altitude) are shown together in Figure 2 and discussed further below.

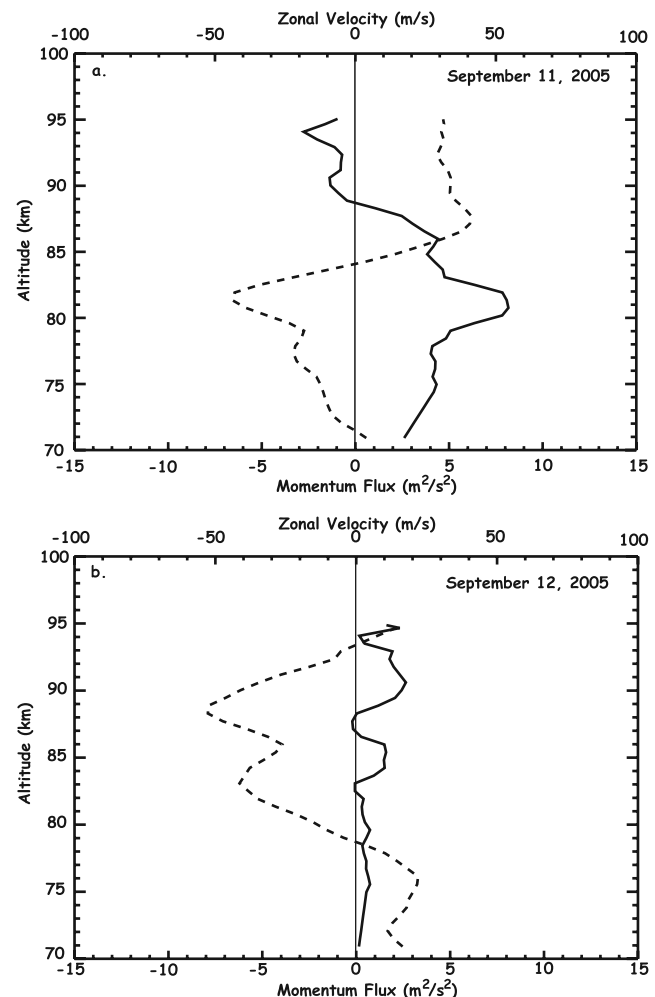


Figure 2. Mean zonal winds (dashed lines) and zonal momentum fluxes (solid lines) averaged for the entire data intervals for (a) 11 and (b) 12 September. The momentum flux profiles were smoothed over 3 km, as that is the minimum vertical GW wavelength that can reasonably be expected to contribute variable momentum fluxes in altitude. No smoothing in altitude was employed for the zonal winds.

[10] Assuming, then, that our momentum flux profiles are valid estimates, we can examine the correlations of the momentum fluxes with the \sim hourly averaged zonal wind profiles. Consider first the last two intervals in Figure 1a having the largest momentum fluxes. In each case, the maximum eastward (positive) momentum fluxes occur where the zonal winds are largest westward (negative) and decrease in magnitude as the zonal wind increases from large negative to large positive values (approximately -50 ms^{-1} to $+50 \text{ ms}^{-1}$). This is exactly the altitude range in which we should expect GWs having eastward phase speeds of ~ 0 to 50 ms^{-1} to experience increasing amplitudes, decreasing intrinsic phase speeds, and an increasing tendency for instability, dissipation, and momentum flux divergence accompanying GW approach to critical levels. Indeed, positive momentum fluxes extended to much higher altitudes in the second to the last interval than in the last interval, suggesting that at least a portion of the GWs accounting for these fluxes had larger zonal phase speeds than in the last profile, where the momentum flux decayed to zero at approximately the altitude where the zonal wind became eastward. Despite indications that GW momentum fluxes reflected primarily modulation and filtering by the zonal winds, they surely also contributed to the observed changes of the zonal wind with time, as the implied accelerations above $\sim 81 \text{ km}$ in the mean profiles are comparable to those expected from the mean GW momentum flux divergence (see Figure 2 below).

[11] We can also estimate the characteristics of the GWs contributing these momentum fluxes, noting that they appear not to propagate significantly beyond the altitude at which the hourly averaged zonal wind is $\sim 50 \text{ ms}^{-1}$ in the 7th profile and $\sim 0 \text{ ms}^{-1}$ in the last profile. Below the strong zonal wind shear, ~ 75 to 82 km , the zonal winds were approximately -30 ms^{-1} and the intrinsic phase speeds were likely ~ 30 to 50 ms^{-1} , with a possible maximum of $\sim 80 \text{ ms}^{-1}$ eastward (based on the altitude extent of the momentum flux in the 7th profile). Assuming midfrequency GWs [Fritts and Alexander, 2003], necessary to account for significant momentum fluxes, the vertical wavelength would have been $\lambda_z \sim 2\pi(c - U)/N \sim 15$ to 25 km for the minimum and maximum phase speeds, assuming a mean buoyancy frequency $N \sim 0.014 \text{ s}^{-1}$. With an apparent dominant period of $\sim 15 \text{ min}$ (a range of ~ 4.5 to 20 min) based on the data in Figure 3 of *Janches et al.* [2006], and a representative horizontal phase speed of 40 ms^{-1} , we estimate a horizontal wavelength (assuming zonal propagation) of $c_{px} T_{GW} \sim (40 \text{ ms}^{-1})(900 \text{ s}) \sim 36 \text{ km}$, where c_{px} is the horizontal phase speed and T_{GW} is the observed GW period. Thus for this GW, the horizontal wavelength would have been ~ 1.5 to 2 times larger than the vertical wavelength, with some spread in this ratio because of the observed spread in periods and likely phase speeds. The horizontal and vertical velocities would have been in the ratio, $u'/w' = \lambda_x/\lambda_z$, and the horizontal velocity contributions to the radial velocities (with $\sin \theta = 0.25$) would have been ~ 30 to 50% of the vertical at $\sim 82 \text{ km}$. This would result in the eastward radial velocities being ~ 2 to 3 times as large as those in the west beam, which appears to be consistent with the data in Figure 3 of *Janches et al.* [2006]. Maximum radial perturbation velocities were $\sim 15 \text{ ms}^{-1}$, with the vertical component accounting typically for ~ 5 to 10 ms^{-1} ,

suggesting horizontal contributions to radial velocities of ~ 2 to 5 ms^{-1} and averaged momentum fluxes as large as ~ 20 to $60 \text{ m}^2 \text{ s}^{-2}$, as observed in the final two profiles in Figure 1a.

[12] Similar arguments can be made about those intervals with significant momentum fluxes on 12 September. These data (Figure 1b) suggest that momentum fluxes were significantly nonzero only during the second and seventh hourly intervals. Note, however, that these statements are based on the assumed validity of \sim hourly averaged zonal velocities and momentum fluxes, and that these assumptions must be reevaluated in light of the S transform momentum flux spectra discussed further below. Despite these caveats, the anticorrelation of the momentum flux and the zonal wind during these times is very clear. In the second interval, the momentum flux began a decrease above $\sim 80 \text{ km}$ toward a negative maximum at and above $\sim 90 \text{ km}$, just where the zonal flow was strongest eastward. Likewise, the momentum flux in the seventh \sim hourly interval exhibited a significant positive maximum extending from ~ 87 to 95 km , just where the zonal flow experienced a strong westward shear with strong westward flow above.

[13] From a broader perspective, we see in Figure 2a that the mean zonal momentum flux for this interval on 11 September is very highly anticorrelated with the mean zonal wind for the same interval, as also noted in a number of previous studies. Looking more carefully, we also note that the GW momentum flux achieves a maximum positive value ($\sim 8 \text{ m}^2 \text{ s}^{-2}$) at the altitude of the most negative mean zonal wind, and that it decreases to small and eventually negative values in the very strong zonal wind shear occurring between ~ 82 and 87 km (a zonal wind change of $\sim 85 \text{ ms}^{-1}$ in only 5 km), and in the sustained strong eastward winds occurring above this shear layer. However, this is exactly what we expect from previous measurements, our estimates of the GW phase speeds provided above, and the extensive modeling and GW parameterization efforts that have been performed to date (see citations above). Indeed, momentum flux magnitudes for this ~ 7 -hour average are consistent with the magnitudes observed in a number of previous measurements and expectations based on large-scale modeling needs (see citations above).

[14] Figure 2b does not allow as simple an explanation, because the zonal momentum fluxes occurring on 12 September tended to be weakly negative (westward) at earlier times and weakly positive (eastward) at later times. Nevertheless, for the interval as a whole, the westward wind shears from ~ 76 to 88 km and the westward mean zonal winds extending to $\sim 93 \text{ km}$ may have played a role in removing those GWs having westward phase speeds preferentially and allowed the tendency for a mean GW spectrum having preferential weak eastward propagation and momentum fluxes extending to the altitude at which the zonal wind again approached zero. The mean eastward momentum flux during the full measurement interval on 12 September was only $\sim 1 \text{ m}^2 \text{ s}^{-2}$, substantially smaller than typical mean values, and arose almost entirely from the single large positive momentum flux profile during the seventh interval, which followed a sustained period of largely westward mean motions. Simply having a conducive propagation environment does not imply large momentum fluxes will occur, however, given the inherent intermittency in GW

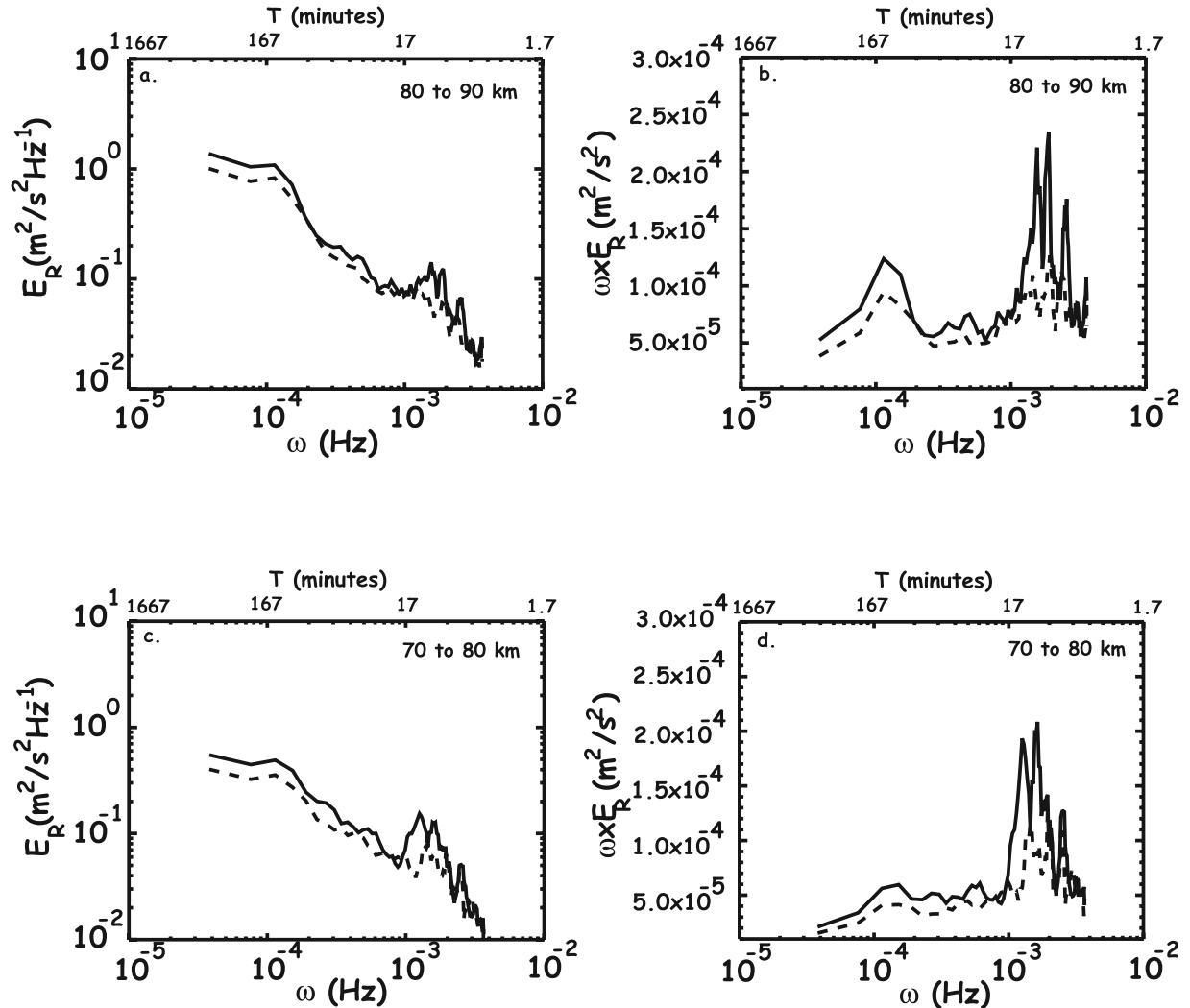


Figure 3. Frequency spectra of radial velocities in standard and “flux-content” form, $\omega E(\omega)$, for all data on 11 September averaged from (a and b) 80 to 90 and (c and d) ~ 70 to 80 km. Solid (dashed) curves indicate eastward (westward) variances, and total variances are proportional to the area under the right hand curves. Periods are shown on the top axis for convenience.

forcing that will be emphasized further below in our S transform analysis.

3. Radial Velocity Frequency Spectra

[15] Frequency spectra of radial velocities were computed for each beam on 11 and 12 September. Because of the momentum flux profiles displayed in Figure 1 above, we have averaged these frequency spectra over altitudes and times appropriate for the major momentum flux measurements in each case. The frequencies referred to in all of our data discussions are observed, or ground-based, frequencies, denoted ω , rather than the GW intrinsic frequencies, ω_i , relative to the local mean horizontal motion, but which require knowledge of propagation directions and horizontal wavelengths for their determination.

[16] Frequency spectra for the entire data interval averaged over altitudes of ~ 71 to 80 and 80 to 90 km on 11 September are shown in Figures 3a and 3c. Similar frequency spectra are shown separately for the first ~ 3 hours

and the last ~ 5 hours averaged over altitudes of 85 to 95 km on 12 September in Figures 4a and 4c. The eastward variances are higher at both altitudes in Figure 3 because of the positive mean momentum fluxes seen in Figure 1. However, Figures 4a and 4b clearly reflect the large negative momentum fluxes in profile 2 on 12 September, while the mean momentum fluxes during the latter intervals were near zero. The reasons for these choices are motivated by the momentum fluxes computed from the radial velocity variances and displayed in Figure 1. While zonal momentum fluxes tended to be zero or positive throughout measurements on 11 September (except at late times and high altitudes, discussed further below), those on 12 September tended to be much more variable spatially and temporally.

[17] Corresponding “variance-content” spectra, $\omega E(\omega)$, in semilog form, are shown in the right panels of each figure, as these exhibit more clearly where the radial velocity variances occur because variance is proportional to the area under the curve in this form. We have also averaged the frequency spectra over five adjacent frequencies (with a

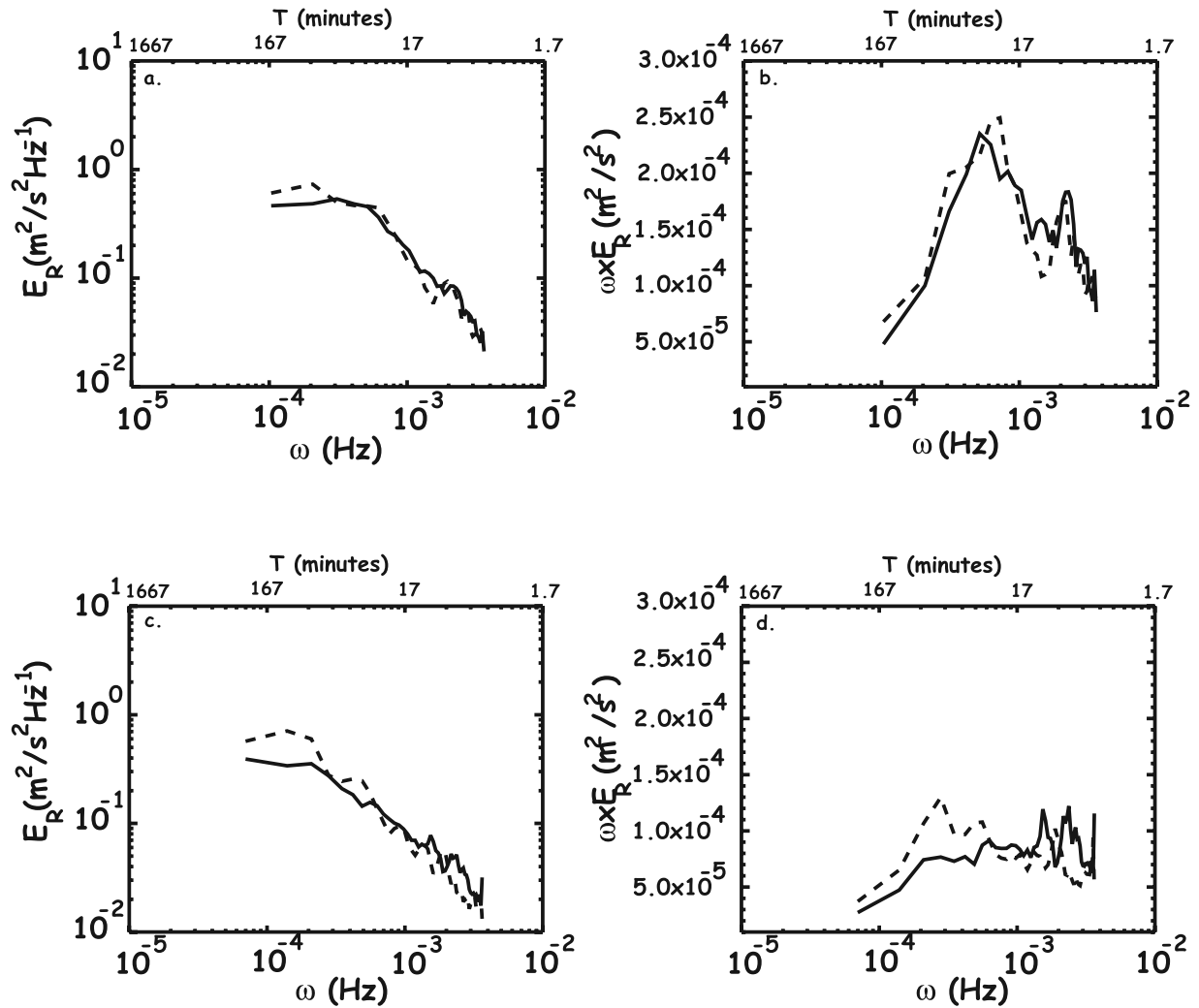


Figure 4. As in Figure 3 but for the (a and b) first three and (c and d) second five intervals on 12 September averaged between 85 and 95 km.

triangular weighting) to allow us to more clearly see the differences between east and west velocity variances. These spectra exhibit different behaviors at lower and higher frequencies. Lower observed frequencies typically correspond to GWs also having lower intrinsic frequencies for which radial winds are dominated by horizontal motions. Higher-frequency GWs, in contrast, result in vertical motions making comparable or larger contributions to radial velocities than horizontal motions. As a result, we expect to see frequency spectra having more negative slopes at lower frequencies (in the standard form), with a flattening, or even reversal (at low wind speeds), of the slope at the highest frequencies [Fritts and VanZandt, 1987; Fritts and Alexander, 2003]. We note, however, a dramatic difference in the character of the frequency spectra, especially as displayed in the “variance-content” forms, between 11 and 12 September that will have important implications to be discussed further below. Despite the very different character of the motion fields and their corresponding frequency spectra on 11 and 12 September, the results for each measurement interval are internally consistent in the sense that the vertical profiles of radial velocity variances computed from the time

series displayed in Figures 2 and 3 of *Janches et al.* [2006], and displayed in Figure 4 (left) of *Janches et al.* [2006], agree completely with those estimated by integrating the frequency spectra at each altitude.

[18] Returning to the frequency spectra themselves, we see in Figure 3 a tendency in both altitude ranges for the largest variances to occur at the highest frequencies, primarily at periods of ~ 4.5 to 20 min, and in the east beam (eastward spectral variances are typically twice westward variances at these highest frequencies). This is the basis for the computation of GW momentum fluxes in sections 4 and 5 below. In Figure 4, we again see that the variances are dominated by the higher frequencies, but in this case the west variances are somewhat larger in the first interval and there are very significant differences in the frequency content of the spectra relative to the data obtained on 11 September.

[19] The data collected on 11 September revealed dominant contributions to radial velocity variances (and zonal momentum fluxes, see below) at periods of ~ 4.5 to 20 min (noted above) and also at periods of ~ 1.5 to 4 hours (with much smaller contributions at intermediate frequencies). In contrast, the spectra obtained on 12 September had compa-

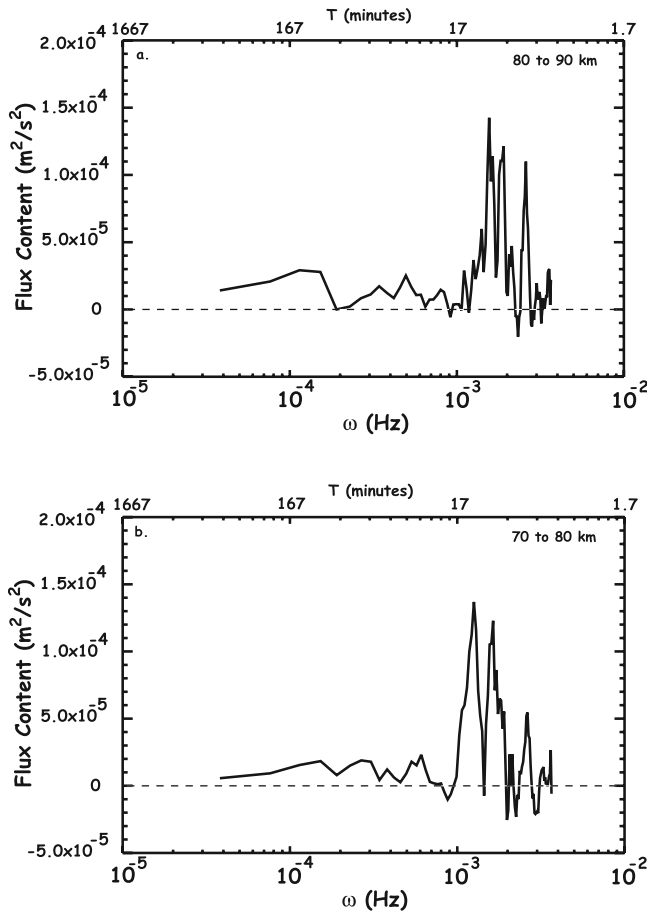


Figure 5. Frequency spectra of momentum flux in “flux-content” form, $\omega\langle u'w' \rangle(\omega)$, for all data on 11 September averaged from (a) 80 to 90 and (b) 70 to 80 km. Positive (negative) values indicate eastward (westward) momentum fluxes, and the total fluxes are proportional to the area under the curves. Periods are shown at the top of each panel.

rable variances (during the first ~ 3 -hour interval) at the highest frequencies, but minimal variances at ~ 1.5 to 3 hours, and instead very high spectral variance at ~ 20 min to 1.5-hour periods (this will be argued below to contribute to momentum flux modulations that are not described by our \sim hourly averaging, but which may, nevertheless, have significant implications for mean and variable GW momentum fluxes and MLT responses).

4. Momentum Flux Frequency Spectra

[20] Momentum flux frequency spectra were obtained by subtraction of west beam from east beam frequency spectra and averaging over those altitudes where the \sim hourly momentum fluxes were large. Specifically, momentum flux frequency spectra were computed for the entire data interval on 11 September and averaged from ~ 71 to 80 and 80 to 90 km. We also performed the same analysis for the first three intervals and the last five intervals on 12 September averaged from 85 to 95 km. This amounts to differencing the variance-content frequency spectra for each group of intervals discussed by

Janches et al. [2006] and above. The resulting momentum flux spectra for 11 and 12 September are shown in “flux-content” form, $\omega\langle u'w' \rangle$, in Figures 5 and 6.

[21] Together with the frequency spectra shown above, the momentum flux spectra emphasize an important point that is often overlooked in assessing GW influences in the lower and middle atmosphere. From these momentum flux spectra, as well as numerous previous studies (see *Fritts and Alexander* [2003] for references), we see clearly that the dominant momentum (and energy) fluxes occur at relatively high frequencies (having smaller energy densities), and specifically far from inertia-GW frequencies (intrinsic frequencies $\omega_i \sim f$, or an inertial period at AO of ~ 38 hours) that contain the majority of the GW energy density because of the typical $\omega^{-5/3}$ (or steeper!) horizontal velocity frequency spectra observed throughout the atmosphere [*Hertzog and Vial*, 2001; *Fritts et al.*, 2006]. It is less clear that higher-frequency GWs dominate the vertical fluxes of momentum and energy at lower latitudes because the low-frequency range of the GW spectrum extends to ever smaller frequencies (and larger energy densities). However,

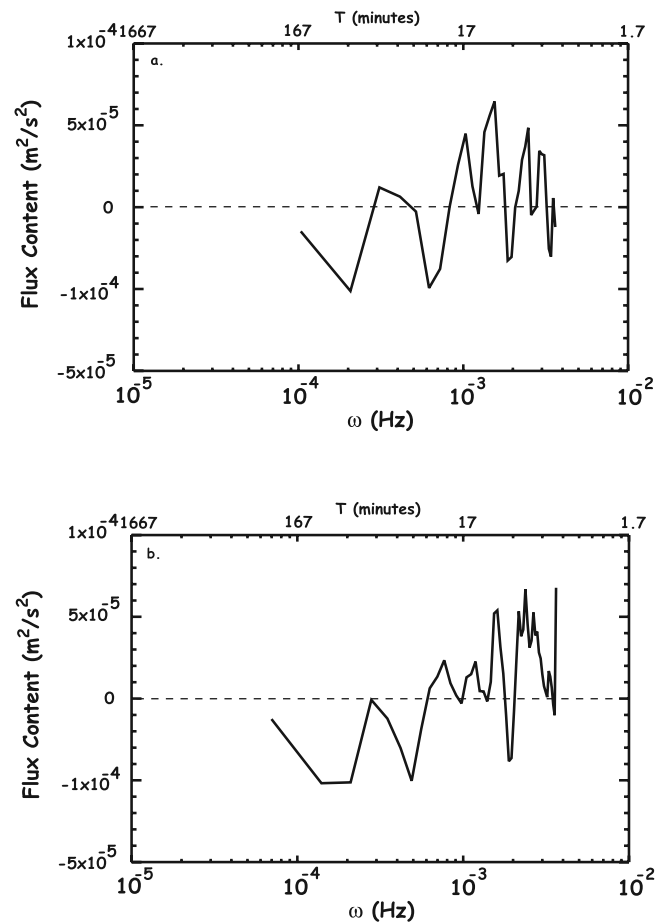


Figure 6. As in Figure 5 but for 12 September 2005 for (a) the first three and (b) the last five intervals averaged over altitudes of 85 to 95 km. Again, the momentum flux spectra confirm the inferences from the radial variance differences displayed in Figure 1. Here, however, the momentum fluxes are largely negative at earlier times but more variable during the end of the measurement interval.

at middle and high latitudes, at least, GW energy densities and their associated momentum (and energy) fluxes occur at essentially opposite ends of the GW frequency spectrum [Fritts *et al.*, 2006], and our focus here is on the contributions of the higher-frequency GWs that we can characterize well with our experimental design at AO. This is also one reason why it is important to be sensitive to GW fluxes (covariances of horizontal and vertical velocity and temperature perturbations) rather than simply GW amplitudes and energy densities. The latter provide the least useful information, while momentum and heat fluxes, their vertical gradients, and their intermittency and dependence on environmental parameters will provide the key insights into the mean and variable forcing of the MLT by GWs.

5. S Transform Frequency and Momentum Flux Spectra

[22] The S transform is a technique employing Gaussian wavelets [Stockwell *et al.*, 1996] for recognizing and quantifying the degree to which oscillations having specific frequencies are localized in time. It is thus ideally suited for our purposes here, as we wish to determine not only the mean forcing of the MLT by GWs, but also the frequencies and the durations of the dominant forcing events and their associated momentum fluxes. MLT GW parameterizations typically assume a large-scale, slowly varying GW forcing that responds primarily to zonal mean and large-scale wind fields. However, the episodic and spatially localized nature of many of the dominant GW forcing events (especially deep convection) and the variable propagation environments encountered by GWs from all sources virtually guarantee that the MLT responses to such events will be far from typical large-scale, slowly varying parameterization assumptions (see Fritts and Alexander [2003] for a general discussion and Vadas and Fritts [2002, 2004] and Fritts *et al.* [2002] for specific examples).

[23] We employ the S transform in this section to both the radial velocity time series and the resulting momentum flux estimates, averaged in altitude and/or time as described above for 11 and 12 September. Radial velocity variances for the east (west) beams are shown with S transforms in Figures 7a, 7c, 8a and 8c (Figures 7b, 7d, 8b, and 8d) for the two measurement intervals, respectively. Figures 7a–7d are for the altitude intervals over which we averaged the frequency spectra in section 3 (~ 70 to 80 and 80 to 90 km on 11 September), while Figures 8a and 8b (Figures 8c and 8d) are for the earlier (later) times on 12 September, both averaged from 85 to 95 km. All S transforms were normalized to the maximum value for that day, independent of beam direction, altitude, or temporal interval. We have also assessed the 99% confidence intervals for all plots, and those contours above zero variance (black) achieve this high confidence when averaged both in altitude and over the temporal width of the Gaussian wavelet employed for each frequency. This does not mean that the radial velocity variance is precise to this degree, but that the S transform has identified the local GW frequency and its associated variance (or momentum flux) within the constraints (the sampling interval, Nyquist frequency, and data quantity) of the available data. In our application of the S transform, we have taken the width of the Gaussian wavelet to be equal to

the wave period being fitted for each period. The S transform spectra are presented in flux-content form in order to show the importance of those frequencies contributing the dominant momentum fluxes.

[24] To establish confidence intervals for the S transform representations of the radial velocity variances and momentum fluxes, we performed estimates of the local power spectrum calculated using a Monte Carlo simulation, employing similar sampling statistics as in our AO measurements. The RMS error of the radial velocity measurements was estimated to be $\sim 1 \text{ ms}^{-1}$, as shown in Figure 4 of Janches *et al.* [2006]. This estimate was obtained by forming an ensemble of normally distributed random variable time series with a standard deviation equal to the estimated error, and the S transform “error” variance was calculated for each realization. The mean S transform error variance indicates the 63rd percentile confidence level (not the 50th percentile, since the distribution of power spectral points is not symmetric about its mean value). The confidence level was then determined by counting the fraction of occurrences of S transform realizations above the noise floor. Different confidence levels are achieved by applying a factor to the noise floor, and it was found empirically that a factor of 3 (4.75) resulted in a 95th (99th) percentile confidence level. The contours above a zero variance value (black contour values) shown in the S transforms of radial velocities and momentum fluxes in Figures 7 and 8 reflect these 99th percentile confidence levels.

5.1. S Transform Frequency Spectra

5.1.1. The 11 September Data

[25] Referring first to the S transform plots in Figure 7, we see evidence of both significant continuity in the large-scale patterns (especially between the east and west beams), but also to a lesser degree between adjacent altitudes and corresponding times in each beam. Comparing first Figures 7a and 7c and Figures 7b and 7d, the lower frequencies (bottom of the plots) have virtually no temporal resolution and simply display the mean variances at ~ 3 to 7-hour periods occurring throughout the ~ 7 -hour measurement interval. There are not significant differences in the apparent low-frequency variances at the lower altitudes. However, there are clear differences at the lower frequencies at 80 to 90 km, i.e., higher eastward than westward variances at frequencies of $\sim 10^{-4}$ Hz and lower (observed GW periods of ~ 3 hours and longer), with a clear variance enhancement in the east beam that corresponds to the eastward enhanced radial velocity spectral variance in Figure 3a and the enhanced positive (eastward) momentum flux seen in the momentum flux spectrum in Figure 5 (primarily Figure 5a) at $\sim 10^{-4}$ Hz and below. As above, the largely positive momentum fluxes agree with the mean momentum fluxes seen in Figure 1 and are surprising in their consistency across all observed frequencies.

[26] The structures seen in the S transforms at higher frequencies on 11 September are much more interesting, as these cannot be captured in the frequency spectra described previously. We first note that high-frequency GW variances and variability appear to occur throughout the ~ 7 -hour measurement interval, but with a general weakening of high-frequency activity from ~ 12 to 14 Arecibo Standard Time (AST), and an even more extended variance depletion

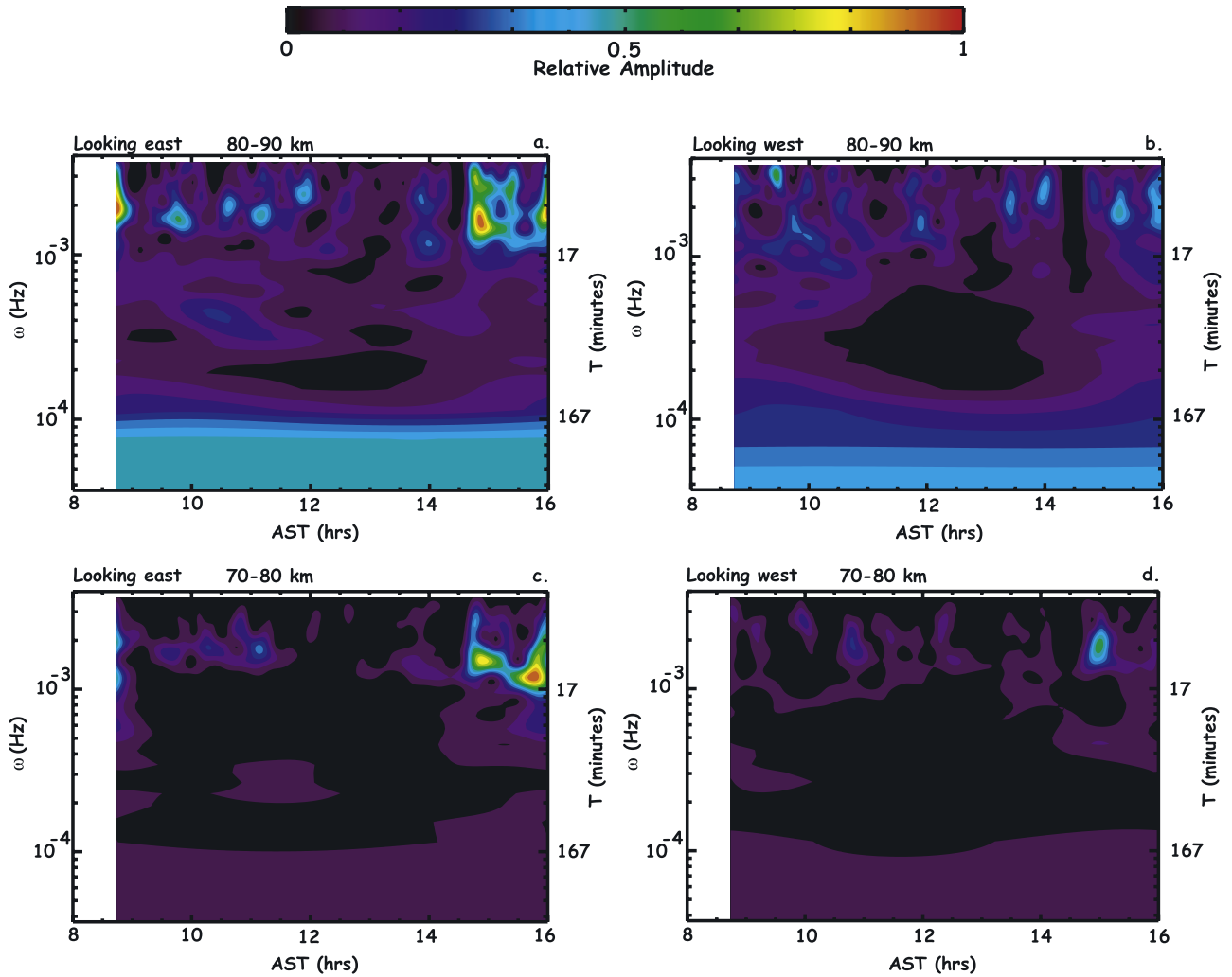


Figure 7. S transforms of the radial wind variance averaged from (a and b) 80 to 90 and (c and d) ~70 to 80 km in the east (Figures 7a and 7c) and west (Figures 7b and 7d) beams for the data collected on 11 September. The variance scale is shown at the top and normalized to a peak value of 1 at the highest variance in the east beam at the highest altitude. The temporal resolution is proportional to GW period, nonzero amplitudes are above the 99% confidence level, and times are Arecibo Standard Time (AST). Periods are shown at the right in each panel.

at intermediate frequencies of $\sim 10^{-4}$ to 10^{-3} Hz (periods of ~ 15 min to 3 hours). As a further reality check, we compare the S transform variances with the radial velocity time series displayed in Figure 2 of *Janches et al.* [2006] and note that there was indeed enhanced high-frequency GW activity at the earlier and later times (note that the S transform data represents only the lower $\sim 80\%$ of those radial velocity data), and that variances were clearly larger after ~ 1440 AST in the east than in the west beam.

[27] The S transform variability at observed periods less than ~ 15 min (clearly not captured by our ~ 52 -min averaged zonal winds and momentum fluxes) is especially significant, with a substantial increase in high-frequency GW variance after ~ 1440 AST and the major response in the east beam in both altitude intervals. Indeed, the close correspondence of the higher-frequency S transform structures in time and frequency are an important confirmation that the two radar beams are indeed sampling largely the same GW field, which is the major requirement to have

confidence in the inferred momentum fluxes employing the dual-beam measurement technique. There is also a suggestion, though it is difficult to quantify, that the GW packet accounting for the relative eastward variance maximum at $\sim 1.5 \times 10^{-3}$ Hz (a period of ~ 10 min) and ~ 1445 AST in Figure 7c was delayed by ~ 10 min in propagating another 10 km in altitude and likely accounts for the somewhat later S transform response at the same frequency and the higher altitude. Indeed, the vertical propagation distance (~ 10 km) and the time delay in the S transform response between the two altitude intervals (~ 10 min) appear generally consistent with the more likely GW period and vertical wavelength (~ 15 min and ~ 15 to 25 km) estimated in section 2 above.

[28] Finally, we note various localized, high-frequency GW packets throughout the east beam, to a lesser extent in the west beam, and to a greater degree at higher altitudes on 11 September. These appear to have typical durations ~ 30 min or less and a typical temporal spacing of ~ 40 min from data onset to ~ 1200 AST. Note also the close correspon-

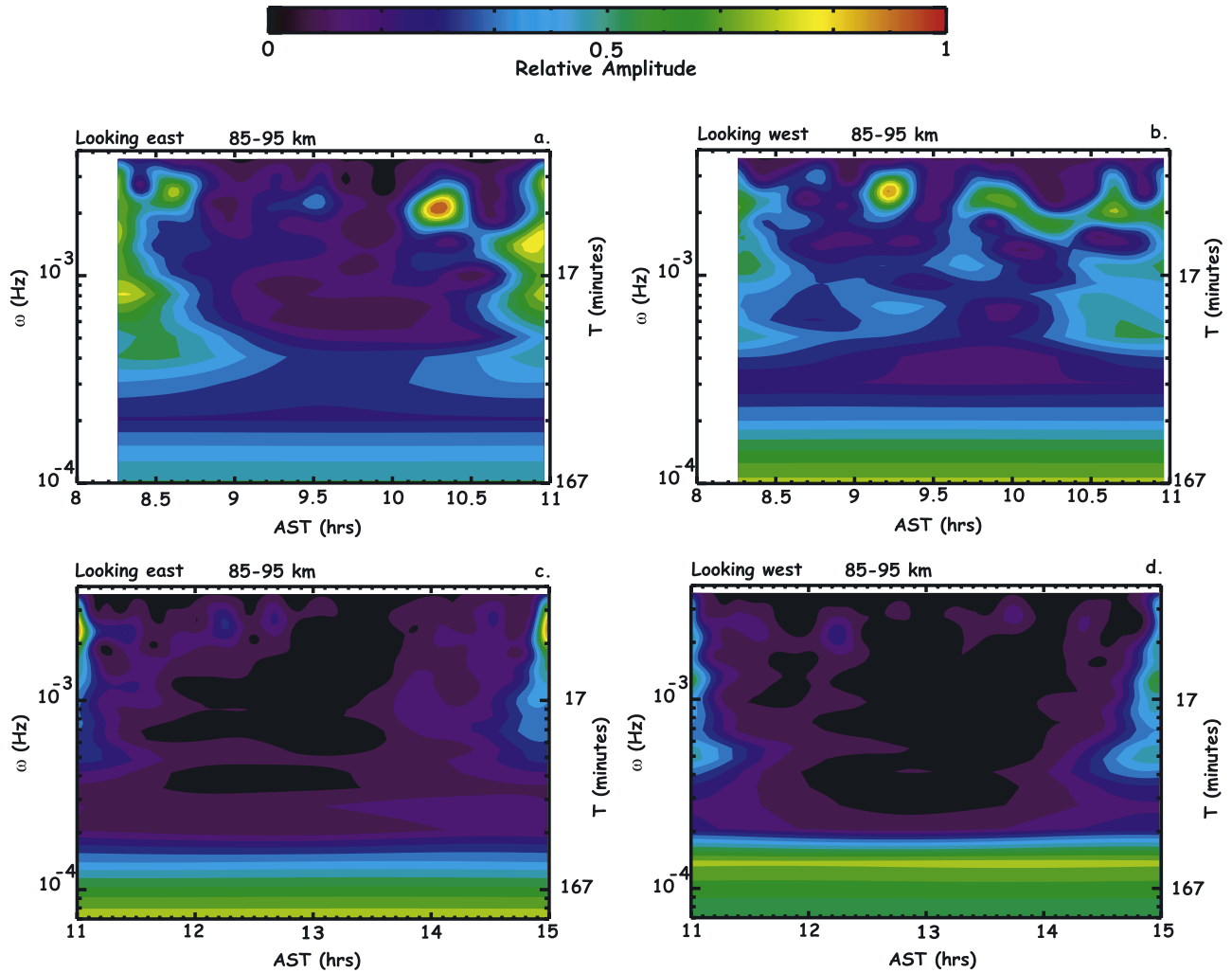


Figure 8. (a–d) As in Figure 7 but for the radial velocity data collected on 12 September. The earlier (later) intervals defined in the text are displayed at the top (bottom).

dence between adjacent altitude intervals, and the comparable observed frequencies where S transform variances are large, especially at ~ 1450 and 1550 AST). Together, these observations and correlations suggest that there are multiple bursts of well-defined, high-frequency, short-duration GW events rather than a slow, systematic presence of, and forcing by, a GW field having the same frequencies, but much less spatial and temporal variability. The clear dominance of the eastward over the westward S transform variances at high frequencies and later times (after ~ 1440 AST) also provides the basis for the substantial \sim hourly mean GW momentum fluxes displayed in Figures 1a and 2a above. However, the much shorter GW packet durations implied by the S transform data displayed in Figure 7 likewise imply significantly larger maximum GW momentum fluxes for the short durations of the GW packets than suggested by the \sim hourly averaged momentum flux profiles shown in Figure 1a. These large estimates are also completely consistent with the large variances and variance differences following the short data gap from ~ 1420 to 1440 AST seen in Figure 2 of *Janches et al.* [2006]. The apparent high temporal variability in GW forcing suggested by these results, and hinted at in previous theoretical

studies, may also contribute to a reconsideration of our basic assumptions in the formulation of improved (and much needed) GW parameterization schemes.

5.1.2. The 12 September Data

[29] The character and details of the S transform were described above and will not be repeated here. However, as above, S transform radial velocity variances have a time resolution proportional to the period of the wavelet being fitted. Thus temporal resolution is low at low frequencies and much higher near our data Nyquist frequency. As seen on 11 September, the low-frequency response on 12 September was relatively uniform across the measurement interval. Unlike 11 September, however, where eastward variances dominated at low frequencies and yielded an eastward (positive zonal) momentum flux at both ~ 70 to 80 and 80 to 90 -km altitude intervals (see Figure 5), westward variances dominated at low frequencies during both the earlier and later measurement intervals on 12 September, resulting in a westward (negative zonal) momentum flux at frequencies of ~ 2 to 3×10^{-4} Hz and below (consistent with the results displayed in Figure 6).

[30] Other aspects of the data collected on 12 September also differed significantly from those discussed above for

11 September. Further evidence of differences between 11 and 12 September comes from the frequency spectra, especially in variance-content form, displayed in Figures 3 and 4. Whereas radial velocity variances on 11 September tended to occur preferentially at periods shorter than ~ 15 min and between ~ 2 to 4 hours, the frequency spectra on 12 September, especially during the earlier averaging interval, exhibited a pronounced and relatively broad variance maximum at periods of ~ 20 min to 1 hour, with significantly smaller variances at the higher and lower frequencies noted on 11 September.

[31] Returning to the S transform data for 12 September (Figure 8), we see that they share some of the common structures between east and west beams noted on 11 September that gives confidence that our assumption of GW field homogeneity between beams remains reasonable. There are also significant S transform variance differences, however, which are related to our assessment of GW momentum fluxes that will be discussed in greater detail below. The radial velocity S transform differences apparently arise because of the very much more variable GW propagation environment on 12 September than on 11 September. The ~ 20 -min to 1-hour radial velocity variance enhancements observed during the earlier interval (Figure 4b) are also apparent in the radial velocity S transforms (Figure 8), where they also exhibit temporal variability that cannot be inferred from Figure 4. The majority of these motions appear to make their major contributions at the earlier and later portions of the first analysis interval, but ~ 15 to 20-min periods appear to play a role throughout this interval. We also judge that the intrinsic frequencies of these GWs are relatively high, given that the S transform variances differ considerably between the east and west beams (hence relatively steep phase slopes). Together, these motions appear to modulate the higher-frequency GWs (periods of ~ 10 min and less) to a high degree, causing them to be strongly filtered and to alter their primary propagation (eastward or westward) on the basis of the lower-frequency GW velocity structures. Indeed, this seems the only possible explanation for the radial velocity S transform variance peaks to oscillate between the east and west beams. It is also suggested by the highly variable momentum flux frequency spectra for 12 September shown in Figure 6, where flux contributions are seen to fluctuate considerably in sign and magnitude. Note, for example, that the ~ 5 to 7-min period motions exhibit maxima in the east beam at times of $\sim 8.6, 9.5, 10.3,$ and 11 AST, whereas west beam maxima occur at $\sim 8.3, 9.2, 9.8,$ and 10.6 AST. This oscillation averages ~ 48 -min and is almost precisely that inferred from the enhanced variance in the frequency and S transform spectra inferred above.

5.2. S Transform Momentum Flux Spectra

[32] We have seen above that S transforms applied to radial velocity data can offer significant insights into the character, propagation anisotropy, potential filtering by, and interactions among different components of the GW motion field that cannot be inferred using more traditional spectral analysis techniques. This is because the wavelet GW description employed within the S transform provides important information on the temporal localization of specific motions, and GW propagation and interactions often

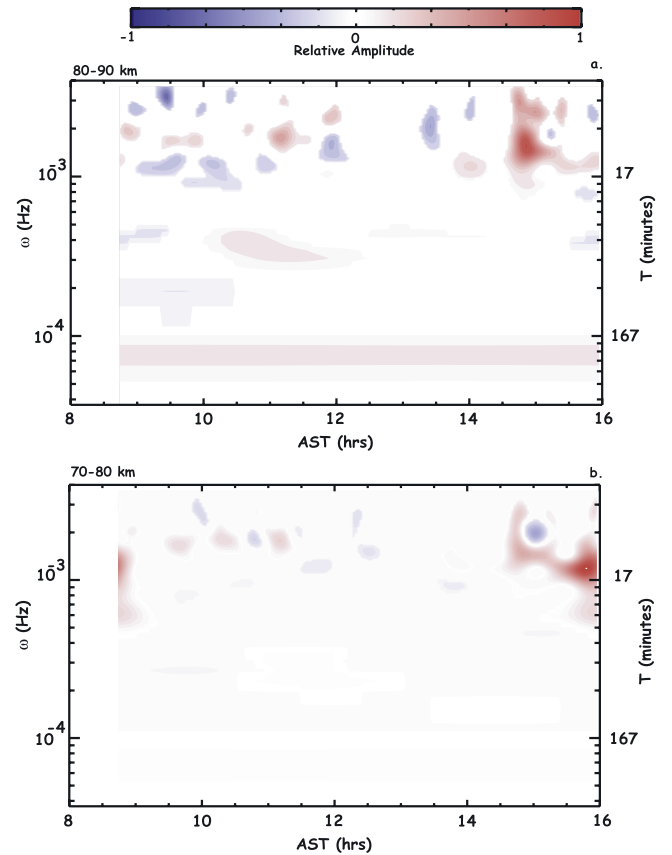


Figure 9. Momentum flux S transforms for the two altitude intervals employed in our evaluation of radial velocity and momentum flux frequency spectra for the data collected on 11 September 2005 for (a) ~ 80 to 90 km and (b) 70 to 80 km. As in Figures 7 and 8, the momentum fluxes are normalized to the maximum magnitude and the current scale includes positive and negative values. White regions in these panels show frequencies and temporal intervals for which momentum flux confidence levels are below 99%. Periods are shown at the right in each panel.

occur on the characteristic GW timescales and have (potentially local and transient) responses that may depend strongly on this temporal localization.

[33] In this section, we take further advantage of the S transform ability to characterize transient responses on the scales of the GW periods to examine the frequencies and the temporal variability of these motions that contribute most to the GW momentum fluxes measured during our measurements intervals at AO. Because the S transform is a linear wavelet decomposition of the field to which it is applied, the S transforms of the GW momentum fluxes for our measurements on 11 and 12 September are simply the differences between the S transform radial velocity variances in the east and west beams on each day. However, the differences emphasize features that were discussed to some extent above in much clearer detail. These data, averaged over the same altitudes and intervals employed in our above discussion, are shown in Figures 9 and 10 for 11 and 12 September, respectively.

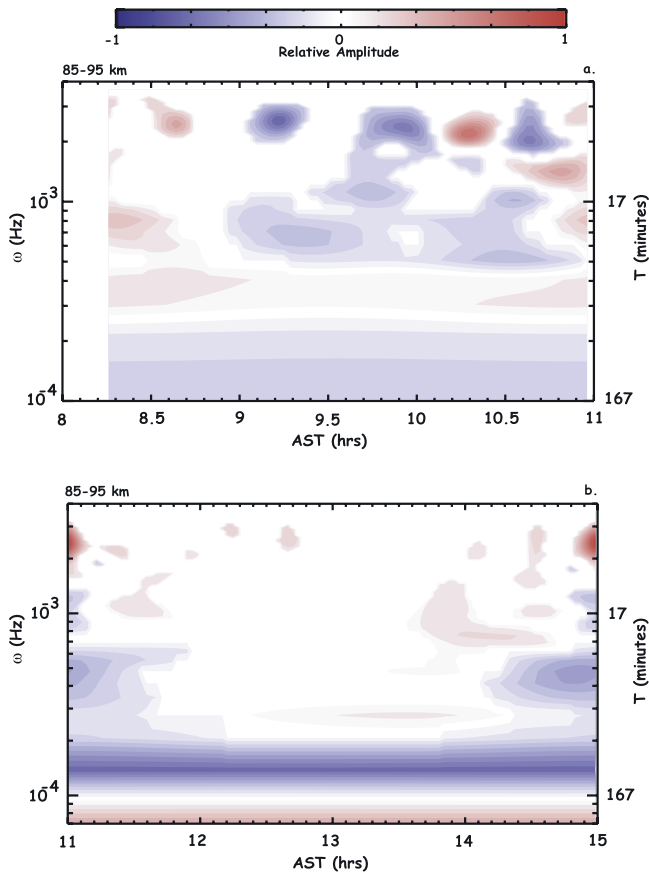


Figure 10. As in Figure 9 but for the momentum fluxes computed for (a) the first three and (b) the second five \sim hourly intervals measured on 12 September 2005.

5.2.1. The 11 September Data

[34] The S transform momentum flux displays for the upper and lower altitude intervals for 11 September are shown in Figure 9. Unlike the S transform radial velocity variances, which exhibit variability on a wide range of timescales, significant momentum fluxes during this interval were confined primarily to the lowest and highest frequencies. As noted above in the discussion of Figures 3 and 5, there was a persistent net positive (eastward) momentum flux at frequencies of $\sim 10^{-4}$ Hz and below, with the greatest contributions at the higher altitudes. What cannot be inferred from the \sim hourly averaged momentum flux profiles or the frequency spectra of radial velocities or momentum fluxes (but which was guessed at from the S transforms of radial velocities discussed above), is the degree to which the high-frequency GW contributions to the total momentum fluxes are composed of relatively discrete events in frequency and in time.

[35] In a relative sense, only a few events appear to contribute significantly to mean momentum fluxes, and these almost certainly dominate the \sim hourly and longer-term averages. There are only three \sim hourly intervals during our measurements on 11 September that we consider to have significant momentum fluxes. A fourth \sim hourly profile (the first) also contains several very large, and a few smaller, momentum flux maxima, but these are typically of opposite sign and largely cancel in the \sim hourly average. The

first significant example (an \sim hourly mean of $\sim 10 \text{ m}^2 \text{ s}^{-2}$) is the third interval averaged from 80 to 90 km and is due largely to the single, temporally localized response at a frequency of $\sim 1.7 \times 10^{-3}$ Hz occurring at ~ 1110 AST in Figure 9a, but with additional positive contributions from lower frequencies ($\sim 5 \times 10^{-5}$ to 10^{-4} Hz and ~ 3 to 5×10^{-4} Hz). A second, and more significant, positive zonal momentum flux averaged from 80 to 90 km (an \sim hourly mean of $\sim 20 \text{ m}^2 \text{ s}^{-2}$) occurred in the second to last interval and included both the low-frequency contribution noted above and a second and much larger contribution at frequencies of $\sim 1.5 \times 10^{-3}$ Hz and above (see the top right corner of Figure 9a). This behavior is hinted at in the momentum flux frequency spectrum shown in Figure 5a; however, the momentum flux frequency spectrum cannot characterize the temporal localization enabled by the S transform. The final example is the very large \sim hourly momentum flux between ~ 70 and 80 km (again achieving an \sim hourly mean of $\sim 20 \text{ m}^2 \text{ s}^{-2}$, but also a peak value of $\sim 60 \text{ m}^2 \text{ s}^{-2}$ at slightly higher altitudes). This large \sim hourly momentum flux arose almost entirely from a single GW event having a frequency of $\sim 1.2 \times 10^{-3}$ Hz (an observed period of ~ 13 min) and a full-width, half-maximum (FWHM) duration of ~ 30 min. Thus the local momentum flux must have been \sim twice as large as the mean value (or $\sim 100 \text{ m}^2 \text{ s}^{-2}$ or larger) over its more limited duration. Indeed, the three examples described here made the major contributions to the daily zonal momentum flux averaged over our measurement interval and displayed in Figure 2a. Remarkably (as suggested by our various analyses above), the dominant GW momentum fluxes, and the body forcings that result when and where these motions undergo dissipation, appear to arise from discrete and spatially localized GW packets that are also often localized in frequency and time. They also contribute momentum fluxes that are comparable to or larger than typical mean values measured at other locations.

5.2.2. The 12 September Data

[36] The S transform momentum flux spectra displayed in Figure 10 for 12 September offers a very different perspective on GW forcing and variability than observed on 11 September. Momentum fluxes on 12 September exhibited significant low-frequency contributions throughout the measurement interval ($\sim 4 \times 10^{-4}$ Hz and below, though note the different minimum frequencies in the two panels because of the different data lengths). Referring to Figure 10a (the ~ 3 -hour interval), we note weak positive momentum fluxes at frequencies of ~ 3 to 4×10^{-4} Hz, but negative momentum fluxes of comparable magnitudes at lower frequencies. These contributions change during the second (~ 5 -hour interval) shown in Figure 10b. In this case, momentum flux contributions tended to be more oscillatory from ~ 2 to 5×10^{-4} Hz (but largely in phase in frequency), with apparently more uniform (because of S transform wavelet bandwidth) momentum fluxes that were large and negative (westward) at ~ 1 to 2×10^{-4} Hz and somewhat weaker and positive at the lower frequencies.

[37] We also observed significant momentum flux variability on 12 September at intermediate frequencies ($\sim 5 \times 10^{-4}$ to 1.5×10^{-3} Hz, or periods of ~ 10 to 30 min), but this was confined virtually entirely to the first ~ 3 -hour

interval. Essentially no momentum flux or variability was noted in this frequency band during the second interval.

[38] At the highest frequencies, we observed both significant variability between the two analysis intervals and within the first, and much more active, interval. The second interval exhibited very little momentum flux or variability worthy of discussion. In contrast, the first interval displayed by far the largest, most variable, and most coherent momentum flux variations we noted during our 2-day experiment. Momentum flux maxima typically extended from ~ 2 to 3×10^{-3} Hz (periods of ~ 5 to 8 min). Both positive and negative maxima achieved magnitudes near the normalized maximum values, but the period of the oscillation of this strong momentum flux modulation was too small not to be averaged over, or strongly aliased, by our \sim hourly zonal wind and momentum flux estimates discussed above. Hence the S transform data presented here offers the only insights into the apparent strong, high-frequency momentum flux modulation that likely arose from modulation of the wind field by the strong ~ 40 -min period GW that also occurred during this interval (and observed in Figure 4b and discussed in sections 3 and 5.1.2 above).

6. Discussion, Summary, and Conclusions

[39] As discussed previously by *Janches et al.* [2006], radial velocity measurements performed during our new daytime application of the AO 430 MHz ISR achieved high accuracy across a range of altitudes extending from ~ 71 to 95 km. Radial velocities (after linear trend removal) achieved amplitudes as large as $\sim 15 \text{ ms}^{-1}$ with uncertainties of $\sim 1 \text{ ms}^{-1}$. The spatial and temporal resolution of these data, and the radial velocity accuracies noted above, enabled a traditional spectral characterization of the GW field in addition to our primary objective: various estimates and characterization of the corresponding GW momentum fluxes. These included \sim hourly zonal wind estimates that exhibited excellent agreement between east and west beams and enabled a characterization of the vertical wave number spectra of the low-frequency portion of the GW field for each \sim hourly profile and the daily means. The latter were found to agree very well with the vertical wave number spectral slopes anticipated from various saturation theories and observed in many previous measurements. Also noted was an apparent mean (downward) vertical velocity measurement bias that showed consistency with previous similar measurements at MLT and lower altitudes, and which, because of our new application of the ISR measurement technique, may assist in the resolution of this current lack in our understanding of radar measurements and mean vertical motions.

[40] The present study extended the analysis by *Janches et al.* [2006] in a number of ways. We computed \sim hourly momentum flux profiles and compared these with the \sim hourly zonal velocities computed for the same intervals. These revealed significant correlations and apparent constraints on the momentum flux profiles by the zonal winds that were found to be in close agreement with previous assessments of these dynamics. The momentum fluxes measured employing this new dual-beam AO application revealed accuracies to be high, given the near-zero magnitudes and profile means when GW activity was not signifi-

cant or highly anisotropic in its propagation. For \sim hourly and daily averages, computed momentum fluxes were comparable to or larger than typical mean values measured at other locations. The ~ 7 -hour mean for 11 September was $\sim 5 \text{ m}^2\text{s}^{-2}$ up to 90 km, while \sim hourly means averaged from ~ 70 to 80 and from 80 to 90 km achieved maxima of ~ 10 to $20 \text{ m}^2\text{s}^{-2}$ (where mean values at a variety of other sites are typically in the range ~ 5 to $15 \text{ m}^2\text{s}^{-2}$ from equatorial to polar latitudes), and the maximum \sim hourly mean reached $\sim 60 \text{ m}^2\text{s}^{-2}$, and was comparable to the largest hourly mean value measured previously. Also noted in the mean profile on 11 September was a strong anticorrelation between the zonal momentum flux and the zonal mean wind, as observed at a number of other sites, and which provides much of the basis for our present crude parameterizations of GW effects in the MLT.

[41] We also computed radial velocity and momentum flux frequency spectra that revealed substantial variability, both in the character (and frequency distribution) of the GW spectrum that contributes to the motion field on any given day, and in the coherence of the momentum fluxes that arise in response to the observed GW field and its environmental modulation and filtering. Mean momentum fluxes on 12 September, in contrast, tended to be significantly smaller, despite comparable mean zonal winds. The GW dynamics on this day were found to be very much different, however, and likely played a large role in the very different responses. While GW responses tended to be relatively systematic on 11 September at low and high frequencies, they were highly variable on 12 September. Indeed, these differing responses provided the motivation for our use of the S transform to examine both radial velocity variances and GW momentum fluxes in section 5 above.

[42] The S transform was described extensively by *Stockwell et al.* [1996] and more specifically for our purposes above. We have employed it here to assess not only the frequency distributions of radial velocities and their implied GW momentum fluxes, but also the temporal variability in the GW field that cannot be captured by traditional spectral methods. This proved to be especially important in highlighting why there were significant differences in the mean GW structures and momentum fluxes on 11 and 12 September, and in pointing to the importance of high variability in the GW motion field and in the implications of interactions among, and filtering by, these motions, in accounting for mean and variable GW influences at MLT altitudes. S transform confidence intervals were assessed and judged to be significant over most of the time and frequency domain at above the 99% significance level.

[43] The S transform results yielded a wide range of insights into the character and variability of the GW field. Specific highlights include (1) the degree to which individual GW motions can be isolated in frequency and time, as this is not at all obvious through inspection of the time series of the radial velocity data shown in Figures 2 and 3 of *Janches et al.* [2006]; (2) the ability to assess GW interactions and filtering that may often occur on timescales smaller than those over which data must often be averaged; and (3) the high degree of discretization (or localization) of the GW field in frequency and time that has been underappreciated in the past, but which will almost certainly have

important implications for our understanding of, and parameterization of, such GW effects in the future.

[44] In future applications of the new AO dual-beam 430 MHz ISR measurement capability, we will attempt to extend measurement durations to cover more of the diurnal cycle, and multiple-day observations, in order to more fully quantify the important, but still largely unknown, mutual interactions among GWs and the mean wind and tidal structures that provide strong modulations of these motions.

[45] **Acknowledgments.** Research support for DCF was provided under NSF grant ATM-0436703, NASA contract NAS5-02036, and AFOSR contract F49620-03-C-0045. Research support for D.J. was provided under agreement 34560-7826 between Cornell University and North-West Research Associates, in which the prime sponsor is NSF under agreement AST-9809484. The Arecibo Observatory is part of the National Astronomy and Ionosphere Center, which is operated by Cornell University under cooperative agreement with the National Science Foundation. Support for D.M.R. was provided under NASA contract NNH05CC70C. Support for R.G.S. was provided by NSF grant ATM-0227885.

References

- Booker, J. R., and F. P. Bretherton (1967), The critical layer for internal gravity waves in a shear flow, *J. Fluid Mech.*, *27*, 513–539.
- Bretherton, F. P. (1969), Momentum transport by gravity waves, *Q. J. R. Meteorol. Soc.*, *95*(404), 213–243.
- Chunchuzov, Y. P. (1971), The interaction of internal waves with the mean wind in the upper atmosphere, *Izv. Atmos. Oceanic Phys.*, *7*, 1090–1092.
- Djuth, F. T., M. P. Sulzer, S. A. Gonzales, J. D. Mathews, J. H. Elder, and R. L. Walterscheid (2004), A continuum of gravity waves in the Arecibo thermosphere?, *Geophys. Res. Lett.*, *31*, L16801, doi:10.1029/2003GL019376.
- Ern, M., P. Preusse, M. J. Alexander, and C. D. Warner (2004), Absolute values of gravity wave momentum flux derived from satellite data, *J. Geophys. Res.*, *109*, D20103, doi:10.1029/2004JD004752.
- Espy, P. J., G. O. L. Jones, G. R. Swenson, J. Tang, and M. J. Taylor (2004), Seasonal variations of the gravity-wave momentum flux in the Antarctic mesosphere and lower thermosphere, *J. Geophys. Res.*, *109*, D23109, doi:10.1029/2003JD004446.
- Espy, P. J., R. E. Hibbins, G. R. Swenson, J. Tang, M. J. Taylor, D. M. Riggan, and D. C. Fritts (2005), Regional variations of mesospheric gravity wave momentum fluxes over Antarctica, *Ann. Geophys.*, *24*, 81–88.
- Fritts, D. C., and M. J. Alexander (2003), Gravity wave dynamics and effects in the middle atmosphere, *Rev. Geophys.*, *41*(1), 1003, doi:10.1029/2001RG000106.
- Fritts, D. C., and T. E. VanZandt (1987), Effects of Doppler shifting on the frequency spectra of atmospheric gravity waves, *J. Geophys. Res.*, *92*, 9723–9732.
- Fritts, D. C., and R. A. Vincent (1987), Mesospheric momentum flux studies at Adelaide, Australia: Observations and a gravity wave/tidal interaction model, *J. Atmos. Sci.*, *44*, 605–619.
- Fritts, D. C., and L. Yuan (1989), Measurement of momentum fluxes near the summer mesopause at Poker Flat, Alaska, *J. Atmos. Sci.*, *46*, 2569–2579.
- Fritts, D. C., L. Yuan, M. H. Hitchman, L. Coy, E. Kudeki, and R. F. Woodman (1992), Dynamics of the equatorial mesosphere observed using Jicamarca MSF radar during June and August 1987, *J. Atmos. Sci.*, *49*, 2353–2371.
- Fritts, D. C., S. L. Vadas, and Y. Yamada (2002), An estimate of strong local body forcing and gravity wave radiation based on OH airglow and meteor radar observations, *Geophys. Res. Lett.*, *29*(10), 1429, doi:10.1029/2001GL013753.
- Fritts, D. C., S. L. Vadas, K. Wan, and J. A. Werne (2006), Mean and variable forcing of the middle atmosphere by gravity waves, *J. Atmos. Sol. Terr. Phys.*, *68*, 247–265.
- Gardner, C. S., K. Gulati, Y. Zhao, and G. Swenson (1999), Measuring gravity wave momentum fluxes with airglow imagers, *J. Geophys. Res.*, *104*, 11,903–11,915.
- Hertzog, A., and F. Vial (2001), A study of the dynamics of the equatorial lower atmosphere by use of ultra-long duration balloons: 2. Gravity waves, *J. Geophys. Res.*, *106*, 22,745–22,761.
- Hitchman, M. H., K. W. Bywaters, D. C. Fritts, L. Coy, and E. Kudeki (1992), Mean winds and momentum fluxes over Jicamarca, Peru during June and August 1987, *J. Atmos. Sci.*, *49*, 2372–2383.
- Janches, D., D. C. Fritts, D. M. Riggan, M. P. Sulzer, and S. Gonzales (2006), Gravity waves and momentum fluxes in the mesosphere and lower thermosphere using 430 MHz dual-beam measurements at Arecibo: 1. Measurements, methods, and gravity waves, *J. Geophys. Res.*, *111*, D18107, doi:10.1029/2005JD006882.
- Kim, Y.-J., S. D. Eckermann, and H.-Y. Chun (2003), An overview of the past, present and future of gravity-wave drag parameterization for numerical climate and weather prediction models, *Atmos. Ocean*, *41*, 65–98.
- Lilly, D. K. (1972), Wave momentum flux—A GARP problem, *Bull. Am. Meteorol. Soc.*, *53*, 17–23.
- McLandress, C. (1998), On the importance of gravity waves in the middle atmosphere and their parameterization in general circulation models, *J. Atmos. Sol. Terr. Phys.*, *60*, 1357–1383.
- Meyer, W., R. Siebenmorgen, and H.-U. Widdel (1989), Estimates of gravity wave momentum fluxes in the winter and summer high mesosphere over northern Scandinavia, *J. Atmos. Terr. Phys.*, *51*, 311–319.
- Murphy, D. J., and R. A. Vincent (1998), Mesospheric momentum fluxes over Adelaide during the 2-day wave: Results and interpretation, *J. Geophys. Res.*, *103*, 28,627–28,636.
- Reid, I. M., and R. A. Vincent (1987), Measurements of mesospheric gravity wave momentum fluxes and mean flow accelerations at Adelaide, Australia, *J. Atmos. Terr. Phys.*, *49*, 4433–4460.
- Reid, I. M., R. Ruster, P. Czechowsky, and G. Schmidt (1988), VHF radar measurements of momentum flux in the summer polar mesosphere over Andenes (69°N, 16°E), Norway, *Geophys. Res. Lett.*, *15*, 1263–1266.
- Smith, A. K. (1996), Longitudinal variations in mesospheric winds: Evidence for gravity wave filtering by planetary waves, *J. Atmos. Sci.*, *53*, 1156–1173.
- Smith, A. K., and L. V. Lyjak (1985), An observational estimate of gravity wave drag from the momentum balance in the middle atmosphere, *J. Geophys. Res.*, *90*, 2233–2241.
- Stockwell, R. G., L. Mansinha, and R. Lowe (1996), Localization of the complex spectrum: The S transform, *IEEE Trans. Signal Process.*, *44*(4), 998–1001.
- Swenson, G. R., R. Haque, W. Yang, and C. S. Gardner (1999), Momentum and energy fluxes of monochromatic gravity waves observed by an OH imager at Starfire Optical Range, New Mexico, *J. Geophys. Res.*, *104*, 6067–6080.
- Tang, J., A. Z. Liu, and G. R. Swenson (2002), High frequency gravity waves observed in OH airglow at Starfire Optical Range, NM: Seasonal variations in momentum flux, *Geophys. Res. Lett.*, *29*(20), 1966, doi:10.1029/2002GL015794.
- Tsuda, T., Y. Murayama, M. Yamamoto, S. Kato, and S. Fukao (1990), Seasonal variation of momentum flux in the mesosphere observed with the MU radar, *Geophys. Res. Lett.*, *17*, 725–728.
- Vadas, S. L., and D. C. Fritts (2002), The importance of spatial variability in the generation of secondary gravity waves from local body forces, *Geophys. Res. Lett.*, *29*(20), 1984, doi:10.1029/2002GL015574.
- Vadas, S. L., and D. C. Fritts (2004), Thermospheric responses to gravity waves arising from mesoscale convective complexes, *J. Atmos. Sol. Terr. Phys.*, *66*, 781–804.
- Vadas, S. L., and D. C. Fritts (2005), Thermospheric responses to gravity waves: Influences of increasing viscosity and thermal diffusivity, *J. Geophys. Res.*, *110*, D15103, doi:10.1029/2004JD005574.
- Vadas, S. L., and D. C. Fritts (2006), Influence of solar variability on gravity wave structure and dissipation in the thermosphere from tropospheric convection, *J. Geophys. Res.*, doi:10.1029/2005JA011510, in press.
- Vincent, R. A., and I. M. Reid (1983), HF Doppler measurements of mesospheric momentum fluxes, *J. Atmos. Sci.*, *40*, 1321–1333.
- Wang, D.-Y., and D. C. Fritts (1990), Mesospheric momentum fluxes observed by the MST radar at Poker Flat, Alaska, *J. Atmos. Sci.*, *47*, 1511–1521.
- Wang, D.-Y., and D. C. Fritts (1991), Evidence of gravity wave–tidal interaction observed near the summer mesopause at Poker Flat, Alaska, *J. Atmos. Sci.*, *48*, 572–583.

D. C. Fritts, D. Janches, D. M. Riggan, and R. G. Stockwell, Colorado Research Associates, NorthWest Research Associates, 3380 Mitchell Lane, Boulder, CO 80301, USA. (dave@cora.nwra.com)

S. Gonzalez and M. P. Sulzer, Arecibo Observatory, National Astronomy and Ionosphere Center, HC3 Box 53995, Arecibo, Puerto Rico 00612.